Thermal-Induced Microstructural Changes of Nickel−Iron Cyanide

C. W. Ng,[†] J. Ding,*[,†] L. Wang,[‡] L. M. Gan,[§,||] and C. H. Quek[§]

Department of Materials Science, National University of Singapore, Singapore 119260, Department of Chemistry, National University of Singapore, Singapore 119260, Department of Physics, National University of Singapore, Singapore 119260, and Institute of Materials and Research Engineering, Singapore 119260

Received: March 7, 2000; In Final Form: July 5, 2000

Molecular-based magnet nickel−iron cyanide, $K_{0.8}Ni_{1.1}[Fe(CN)_6]\cdot 4.5H_2O$, was prepared by coprecipitation. The powder X-ray diffraction indicates an fcc crystal structure with a unit cell constant of 10.4 Å. Its Curie temperature was determined to be 28 K from the Curie−Weiss law. The effects of heat treatment on the microstructures as well as magnetic properties in the compound were studied. Several structures were encountered during the course of annealing from room temperature to 600 °C. The conversion of the ferromagnetic Fe^{III}−CN−Ni^{II} linkage to a paramagnetic Fe^{II}−CN−Ni^{III} linkage occurred after heat treatment at 150 °C in argon. There was another cyanide structure with a tentative composition of $(Ni, Fe)(CN)_{2-3}O_{1-2,}$ which possessed a Curie temperature of 50−60 K and is expected to be ferrimagnetic. Above 550 °C, the cyanide compound decomposed into a mixture of fcc Fe−Ni and amorphous carbon. In a separate experiment, fairly pure fcc Fe−Ni particles were prepared by microemulsion method followed by decomposition at 600 °C under a partial pressure of air. The ultrafine particles were found to have a mean particle size of ∼10 nm, a saturation magnetization of 110 emu/g, and a coercivity of 0.3 kOe.

I. Introduction

Molecular magnetism is a field that has developed rapidly in the past few years.[1−5,14,15] Among other reasons, this situation is due to the fact that this field lies at the meeting point of three separated disciplines, namely, molecular materials, bioinorganic chemistry, and magnetism. The search for molecule-based ferromagnets having Curie temperature T_c at or above room temperature is the major driving force in the field, in search of magnets with lower weight and good chemical stability.[6−8] There are other important challenges such as the design and characterization of mesoscopic molecules possessing large magnetic moments, the study of molecules exhibiting spin crossover phenomena, and the search for materials combining two or more functional properties, e.g., magnetooptics, superconductivity, and magnetism,[10−13] etc.

Among many compounds in molecular-based ferromagnets, the cyanide complex is one of the most promising candidates for applications as lightweight magnets because of its high Curie temperature values.[11−13] In this research work, the mixed-metal system using hexacyanometalates, i.e., octahedral $[M(CN)_6]^{n-}$, as the molecular building blocks has been investigated. Owing to its strong electron-withdrawing ability, the cyanide ligand (CN−) tends to induce π-back-bonding into the $2p\pi^*$ orbital, which is antibonding in nature. It is this strong π-acceptor nature of CN^- that makes M (Fe^{III} or Fe^{II} ions, in this case) stay as low-spin.[9] The cation (Ni^{II} or Ni^{III}, in this case) always remain as high-spin.

Nanoscale magnetic particles have many unique electrical, chemical, structural, and magnetic properties, with potential applications in information storage, color imaging, catalysis, bioprocessing, magnetic refrigeration, and ferrofluids.[16] Among the methods for producing nanomaterials, the coprecipitation technique has been applied in this work for its simplicity in preparation.

The motivation of this research work is to characterize the physical and chemical as well as the magnetic properties of these molecular magnets in order to explore their potential as the next-generation magnet.

II. Experimental Methods

The material being investigated was nickel−iron cyanide-based Prussian blue analogue. It can be represented by the formula $K_xM_y^{2+}[Fe^{3+}(CN)_{6-}]_2^{3-}\cdot nH_2O$, where M = Ni. The reaction of $K_3Fe^{III}(CN)_6$ (0.43 M) and $Ni^{II}(NO_3)_2$ (0.83 M) in aqueous solution produced a light brown precipitate. Chemical microanalysis yielded the formula $K_{0.8}Ni_{1.1}[Fe(CN)_6]\cdot 4.5H_2O$. This coprecipitated powder was annealed at different temperatures (100, 150, 200, 400, and 600 °C) for 2 h under pure argon atmosphere, to study the possible effect of annealing on its structural and magnetic properties. One sample was annealed at 200 °C for 2 h in air, to form a metastable structure.

Thermogravimetric analysis (DuPont TGA 2950) and differential scanning calorimetry (DuPont DSC 2910), powder X-ray diffraction (Siemens XRD 5500) using Cu−Ka_1 radiation, transmission electron microscopy (JEOL-100CX), and Fourier transform infrared spectroscopy (Bio-Rad FTS 135) were used to characterize the physical and chemical properties of the materials. The magnetic properties were investigated using vibrating sample magnetometer (Oxford 90 kOe VSM), measured up to 50 and 90 kOe at variable temperatures, depending on the necessity of the sample. Mössbauer spectroscopy (Ranger Scientific MS 1200) was also used to probe the magnetic properties in the temperature range of 4 K to room temperature. Magnetic susceptibility χ was determined from the magnetiza-

[†] Department of Materials Science, National University of Singapore.
[‡] Department of Physics, National University of Singapore.
[§] Department of Chemistry, National University of Singapore.
[||] Institute of Materials Research and Engineering.

10.1021/jp000881w CCC: $19.00
Published on Web 08/31/2000

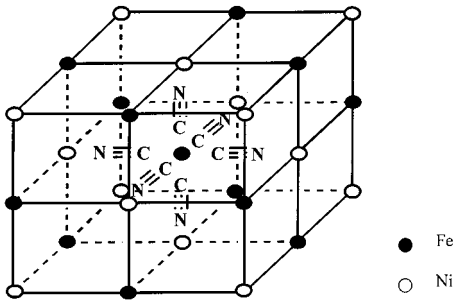

Figure 1. Fcc structure of Fe−Ni cyanide. For simplicity and clarity, the K^+ ions and coordination water molecules have been omitted. The solid and dotted lines represent the cyanide (CN−) bonds. In an ideal cubic structure, each Fe ion is bonded to a carbon atom while each Ni ion is bonded to a nitrogen atom.

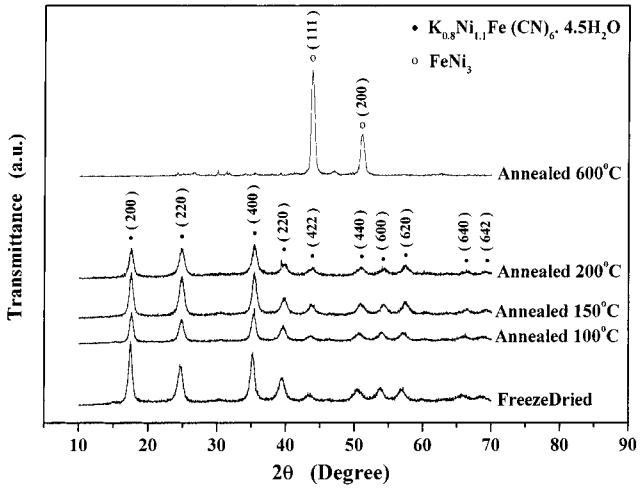

Figure 2. Powder XRD diffractogram of (a) various Ni−Fe cyanides annealed in argon atmosphere at different temperatures; (b) Ni−Fe cyanide annealed in air at 200 °C.

tion/field slop at low magnetic fields (typically in the range of 100−1000 Oe).

III. Results and Discussion

A. Powder X-ray Diffraction (XRD). The crystal structure of $K_{0.8}Ni_{1.1}[Fe(CN)_6]\cdot 4.5H_2O$ was referred from powder X-ray diffraction data.[19] The Fe and Ni ions are octahedrally coordinated by C and N atoms, respectively, forming three-dimensional bimetallic networks with the CN^- (cyanide) groups as the bridging ligands. The impurity atoms such as K^+ ions may occupy the interstitial sites in the cubic crystal lattice.[9] A schematic representation of the compound is shown in Figure 1.

TABLE 1: Summary of Some Physical Parameters, a_0 and a_0^3, of Various Ni−Fe Cyanides Treated at Different Temperatures

treatment	lattice parameter a_0 (Å)	unit cell volume a_0^3 (Å^3)
freeze-dried	10.41	1128.8
annealed 100 °C (in argon)	10.42	1132.0
annealed 150 °C (in argon)	10.22	1065.9
annealed 200 °C (in argon)	10.20	1060.3

Figure 2 compares the powder XRD pattern of as-coprecipitated (freeze-dried) sample to those of coprecipitation-derived samples of Ni−Fe cyanides treated at different thermal temperatures under argon atmosphere. For the as-coprecipitated sample, all the diffraction peaks can be identified with the fcc structure, as expected for Ni−Fe cyanide.[12] The lattice parameter a_0 was determined to be 10.41 Å. The results are nearly identical to that reported previously.[18]

Samples annealed at 100, 150 and 20 °C in argon have the fcc structure as well. Their lattice parameters are listed in Table 1. In comparison with the freeze-dried sample, no significant change was found for the sample after annealing at 10 °C. After heat treatment at 150 and 200 °C, the lattice parameter a_0 reduced approximately 2% accompanied by a significant decrease in the unit cell volume. The changes in lattice parameter and unit cell volume indicate a possible change in structure.

Figure 3 shows the TEM micrograph of the freeze-dried sample. The sample consists of nanosized particles with mean particle size of around 10 nm. By using the Scherrer formula, the calculated crystallite size from the XRD peaks was 10−15 nm, which is in good agreement with the TEM result. During the TEM study, all the electron diffraction rings could be well described with the fcc structure of the Ni−Fe cyanide.

The TEM study showed no significant change of particle size and particle morphology after annealing the cyanide at 150 and 200 °C. However, the line broadening found in the XRD peaks

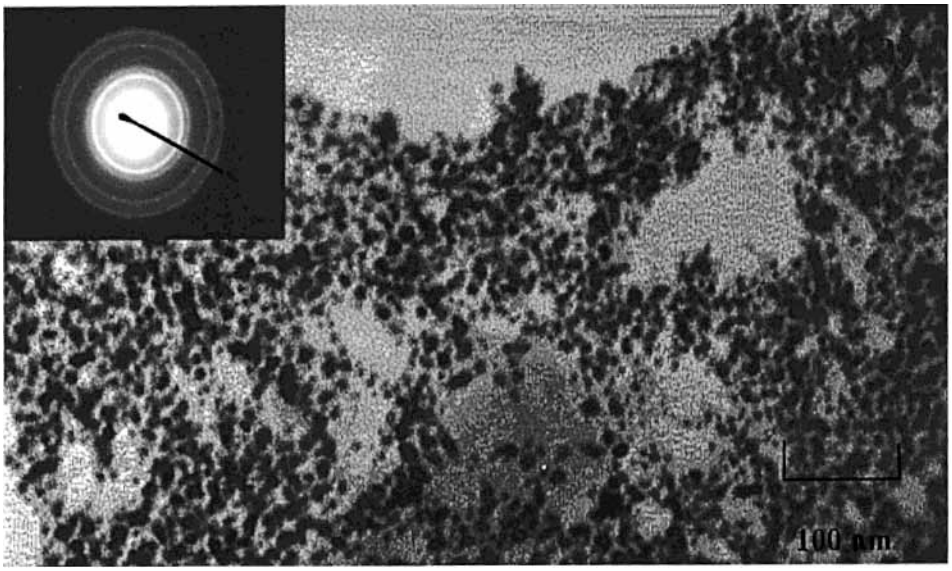

Figure 3. TEM micrograph of freeze-dried sample of Ni−Fe cyanide. The inset on the top left corner showed the diffraction rings corresponding to the cyanide particles.

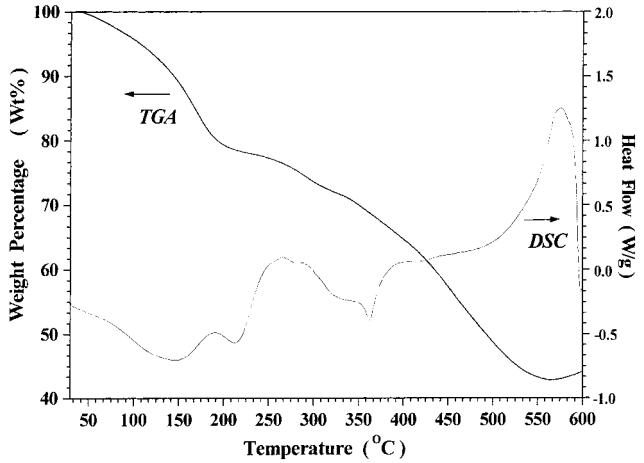

Figure 4. Thermogravimetric analysis (TGA) and differential scanning calorimetry (DSC) spectrum of freeze-dried Fe−Ni cyanide, $K_{0.8}Ni_{1.1}[Fe(CN)_6]\cdot 4.5H_2O$.

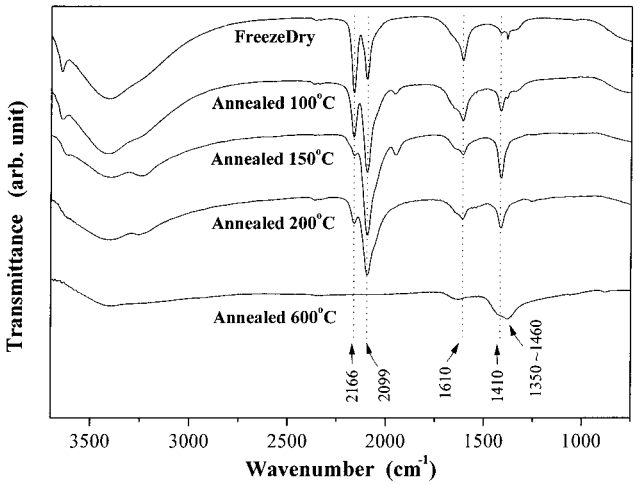

Figure 5. Fourier transform infrared (FTIR) spectrum of Ni−Fe cyanide treated at various temperatures. The peaks indicated at 2166 and 2099 cm^{-1} correspond to the CN stretching in $Fe^{III}-CN-Ni^{II}$ linkage and $Fe^{II}-CN-Ni^{III}$ linkage, respectively. The peak at 1410 cm^{-1} is the CN stretching in the structure $(Ni^{II}-Fe^{III})\cdot(CN)_{2-3}O_{1-2}\cdot$Fe−Ni stretching was observed in the range of 1350−1460 cm^{-1}, while that of O−H bending was at 1610 cm^{-1}.

(Figure 2) of the two samples was larger than that of the freeze-dried powder. This again suggested possible microstructural changes after the annealing.

After being annealed at 400 °C, the peaks corresponding to the fcc Fe−Ni phase began to show up. Further annealing beyond 550 °C caused the decomposition of the Fe−Ni cyanide. This was concluded from the XRD pattern in Figure 2, wherein high-intensity peaks corresponding to the Fe−Ni particle were observed.

B. Thermogravimetric Analysis (TGA) and Differential Scanning Calorimetry (DSC). From the chemical microanalysis, the freeze-dried powder has a chemical composition of $K_{0.8}Ni_{1.1}[Fe(CN)_6]\cdot 4.5H_2O$ (relative molecular mass = 385.5 g/mol). The following annealing processes were done in inert nitrogen atmosphere. After annealing at 150 and 200 °C, respectively, the number of water molecules was reduced from 4.5 to below 1, indicating a loss of water molecules. After heat treatment at 400 °C, the concentration of nitrogen was significantly reduced with a possible composition of $(Ni, Fe)(CN)_{2-3}O_{1-2}$ for the cyanide compound. After heat treatment at 550 °C, only metallic and carbon particles were left. This result showed that decomposition was not completed after annealing at 400 °C. Carbon remains in the sample after decomposition, probably in the form of amorphous carbon, because no crystalline phases related to carbon-containing phase were found in the XRD patterns (Figure 2).

Figure 4 shows the TGA and DSC measurements of the coprecipitation-derived iron−nickel cyanides, from room temperature to 600 °C in an inert nitrogen atmosphere. In TGA, each slope (step) infers a loss of weight of the compound within a different temperature range. Hence, the initial three steps in TGA correspond to water loss processes. The first step between room temperature and 100 °C (percentage weight loss, percent weight loss ≈5%) corresponds to the loss of about one water molecule per unit formula. The second step, from 100 to 175 °C (percent weight loss ≈15%), corresponds to the loss of the three water molecules. Beyond 175 °C the loss of the rest of the half water molecule took place. These deductions are in fact well supported by the chemical microanalysis results. The further step in the temperature range of 200−550 °C corresponds to the decomposition of the cyanide phase. The remaining weight at 550 °C can be well described by the loss of all the water molecules and all the nitrogen atoms.

In the DSC curve, the endothermic curves (concave curve) below 20 °C in the DSC indicate loss of water molecules. The exothermic curves (convex curve) correspond to the decomposition processes. The broad DSC peaks (in the range of 230−33 °C) might be associated with the possible microstructural changes related with the volume expansion (Table 1) and partial decomposition of the cyanide compound beyond 250 °C. Complete decomposition occurred around 550 °C, whereby iron−nickel phase was found with a significant amount of pure carbon particles (≈15 wt %) and practically no nitrogen by chemical microanalysis, as a consequence of the breakdown of the cyanide groups in the cyanide sample.

C. Fourier Transform Infrared Spectroscopy (FTIR). The microstructural changes observed in XRD, TGA, and DSC were confirmed by FTIR spectroscopy. The FTIR spectra for the coprecipitation-derived Ni−Fe cyanide samples in the freeze-dried state and after annealing at different temperatures are illustrated in Figure 5. All the peaks related to the different cyanide structures are in the range of 1400−2200 cm^{-1}. The peaks above 3000 cm^{-1} correspond to the O−H stretching of lattice water molecules.

In the FTIR spectrum of the freeze-dried sample, two prominent peaks were observed at 2166 and 2099 cm^{-1}. Other than these two peaks, there is one appearing at 1610 cm^{-1} and another weak peak at 1410 cm^{-1}. According to ref 11, the peak at 2166 cm^{-1} corresponds to the CN stretching in $Fe^{III}-CN-Ni^{II}$ linkage, while the peak at 2099 cm^{-1} is due to the CN stretching in $Fe^{II}-CN-Ni^{III}$ linkage. Annealing at 100 °C resulted in a decrease of the intensity of the peak at 2166 cm^{-1} relative to that at 2099 cm^{-1}. After annealing at 150 °C, the peak at 2166 cm^{-1} nearly disappeared. The FTIR spectrum of the sample annealed at 200 °C was much the same as that of the sample annealed at 150 °C. This result has shown that the two cyanide linkages ($Fe^{III}-CN-Ni^{II}$ and in $Fe^{II}-CN-Ni^{III}$) coexisted in the freeze-dried state. Heat treatment results in dehydration, as detected by TGA and DSC and chemical microanalysis as discussed before, which is accompanied by conversion of the $Fe^{III}-CN-Ni^{II}$ linkage to the $Fe^{II}-CN-Ni^{III}$ linkage as suggested by the FTIR study. It is worth noticing the reduction of the lattice parameters in Table 1, which is certainly associated with the bonding linkage conversion.

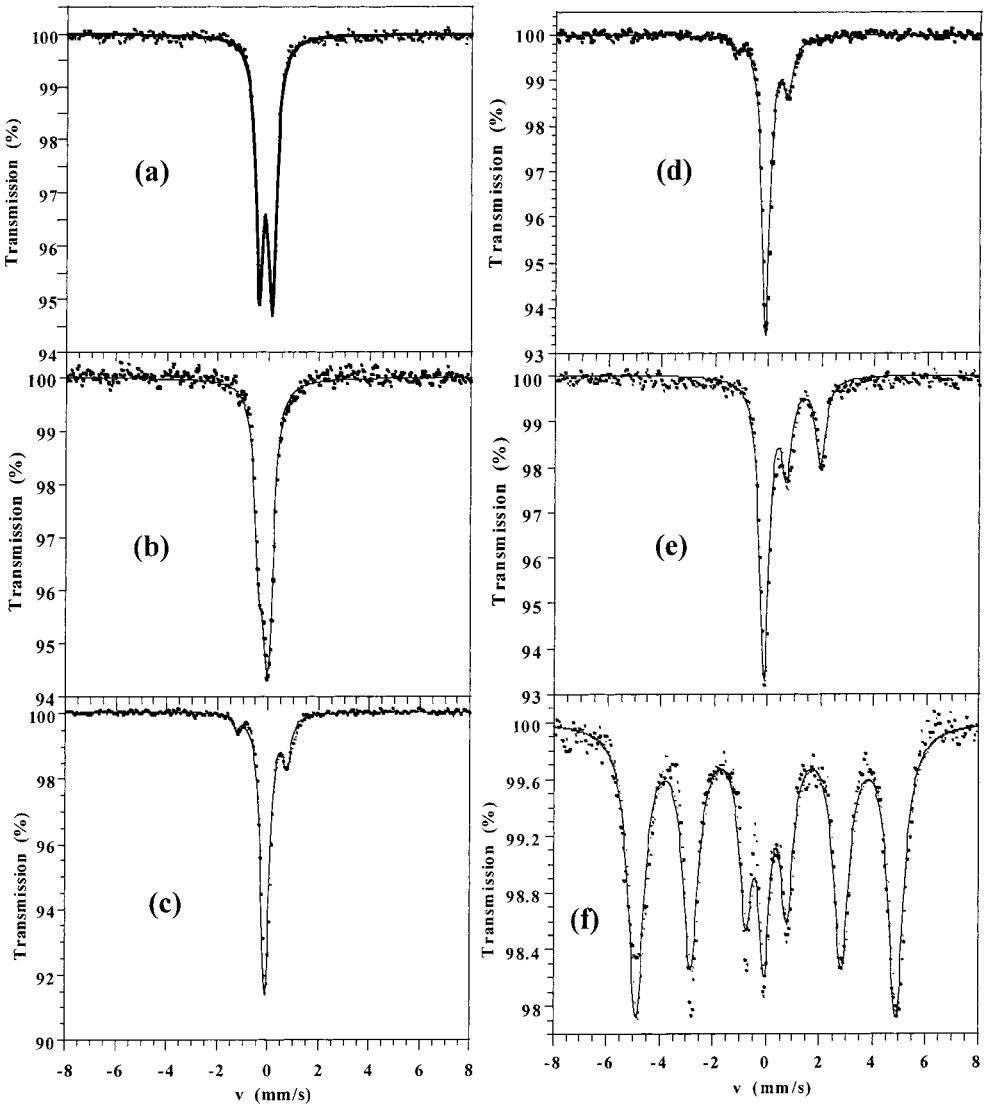

Figure 6. Room-temperature Mössbauer spectra of Ni−Fe cyanides under different thermal treatments: (a) freeze-dried; (b) annealed 100 °C; (c) annealed 150 °C; (d) annealed 200 °C; (e) annealed 400 °C; (f) annealed 600 °C.

TABLE 2: Illustration of the Chemical Shift (CS), Quadrupole Splitting (QS), and Hyperfine Field (HF) of the Different Structures during Different Stages of Thermal Treatment

	temperature (K)							
	290			77			4	
chemical formula	CS (mm/s)	QS (mm/s)	HF (kOe)	CS (mm/s)	QS (mm/s)	HF (kOe)	CS (mm/s)	HF (kOe)
$(K_{0.8}Ni^{II}_{1.1}Fe^{III})(CN)_6$	0.15	0.54		0.06	0.87		0.13	268
$(K_{0.8}Ni^{III}_{1.1}Fe^{II})(CN)_6$	0.13			0.03			0.15	
$(K_{0.8}Ni_{1.1}Fe)(CN)_{2-3}O_{1-2}$	0.35	0.68		0.42	0.95		0.49	493
$(K, Ni, Fe)(CN)_x$ $(x < 2)$	1.36	1.28		1.60	1.57			
fcc FeNi	0.02		303	0.04		301		

As the annealing temperature was increased, there is another peak at 1410 cm^{-1} that became more and more prominent. This peak could be due to another type of linkage, which probably has the composition of $(Ni, Fe)(CN)_{2-3}O_{1-2}$ as concluded from chemical microanalysis. The presence of this linkage was further verified by the Mössbauer spectroscopy (discussion later) on Ni−Fe cyanide annealed in air at 200 °C, which comprised 94% of this linkage in the compound.

After annealing at 250 and 400 °C, respectively, the peak at 2099 cm^{-1} shifted to lower wavenumber. The shift is related to the partial decomposition of cyanide bonds beyond 250 °C, leading to disordered structure. After annealing at 600 °C, there is a broad peak in the region 1350−1460 cm^{-1}. The peak corresponds to the Fe−Ni stretching, as the fcc Fe−Ni phase was formed after the decomposition of the cyanide compound.

The peak at 1610 cm^{-1} was well-known to be the O−H bending arising from the water molecules embedded in the cyanide crystal lattice. The intensity of the peak decreases strongly after annealing at 150 °C, confirming the dehydration. However, the sample after dehydration is highly hygroscopic, so the remanent O−H peaks were due to the absorption of atmospheric water during the sample preparation and FTIR measurements.

TABLE 3: Quantities of the Various Structures Present in the Samples under Different Thermal Treatments Measured by ^{57}Fe Mössbauer at 290 K

	structures				
thermal treatment	$Fe^{III}-CN-Ni^{II}$	$Fe^{II}-CN-CN^{III}$	$(Ni, Fe)(CN)_{2-3}O_2$	$(Ni, Fe)(CN)_x$ ($x < 2$)	fcc FeNi
freeze-dried	92%	8%			
annealed 100 °C (in argon)	60%	40%			
annealed 150 °C (in argon)	5%	90%	5%		
annealed 200 °C (in argon)	4%	88%	8%		
annealed 400 °C (in argon)		40%		60%	
annealed 600 °C (in argon)				10%	90%
annealed 200 °C (in air)		6%	94%		

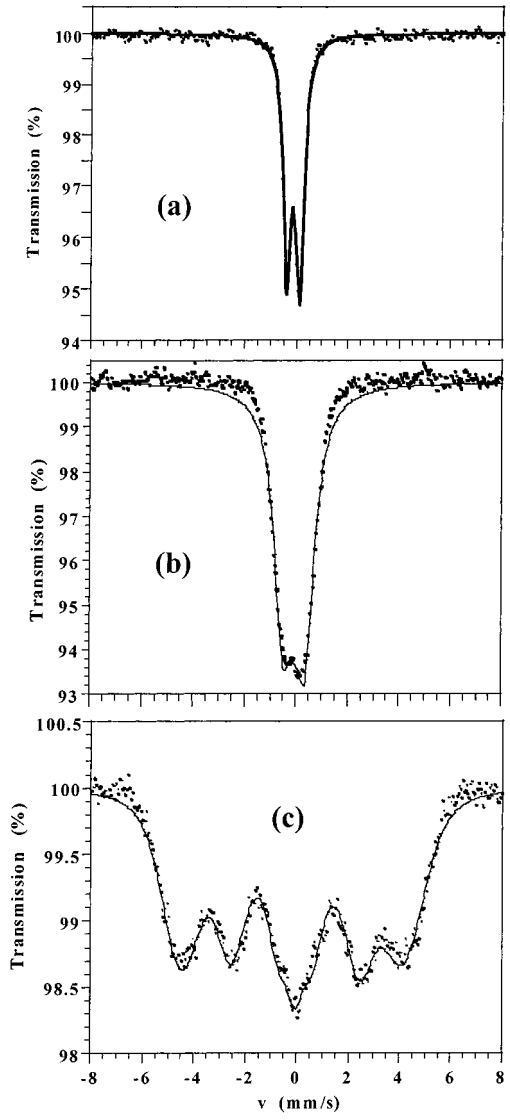

Figure 7. Mössbauer spectra of freeze-dried sample measured at three different temperatures: (a) 290 K; (b) 77 K; (c) 4 K.

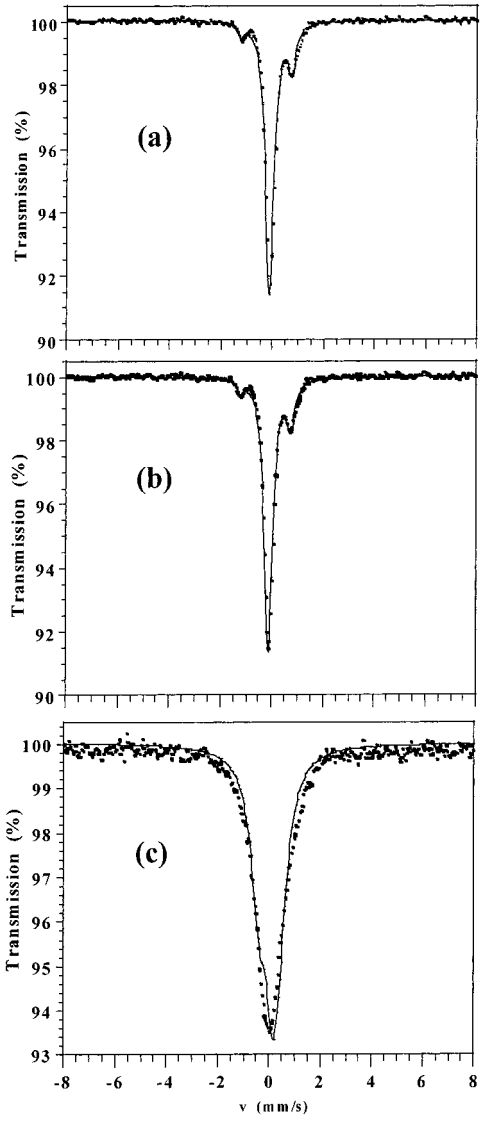

Figure 8. Mössbauer spectra of sample annealed at 15 °C in argon measured at three different temperatures: (a) 290 K; (b) 77 K; (c) 4 K.

In conclusion, the cyanide powder consists of two structures, namely the $Fe^{III}-CN-Ni^{II}$ linkage (majority) and the FeII−CN−NiIII linkage, in the freeze-dried state. Heat treatment up to 200 °C leads to the conversion of $Fe^{III}-CN-Ni^{II}$ linkage to the $Fe^{II}-CN-Ni^{III}$ linkage, since the peak corresponding to the $Fe^{III}-CN-Ni^{II}$ linkage disappears after annealing at 150 and 200 °C. Another cyanide linkage as suggested by (Ni, Fe)$(CN)_{2-3}O_{1-2}$ from the chemical microanalysis arose after heat treatment. Only peaks correspond to the presence of Fe−Ni particles appeared in samples annealed beyond 550 °C.

D. Mössbauer Spectroscopy. As expected, the magnetic properties of these Ni−Fe cyanides (whether heat-treated or not) are influenced directly by the symmetry of the cubic crystal field. This aspect was probed in detail by using ^{57}Fe Mössbauer spectroscopy. The FTIR spectrum shown earlier gave the two structures involving different iron valencies, but only qualitatively. The Mössbauer spectrum, on the other hand, gave the quantitative results.

The room-temperature ^{57}Fe Mössbauer spectra of the Ni−Fe cyanides under different thermal treatments are shown in Figure 6a−f. In the freeze-dried sample, majority of the spectrum consisted of a doublet, with a minor amount of a singlet. The quantity of the doublet decreased significantly in comparison

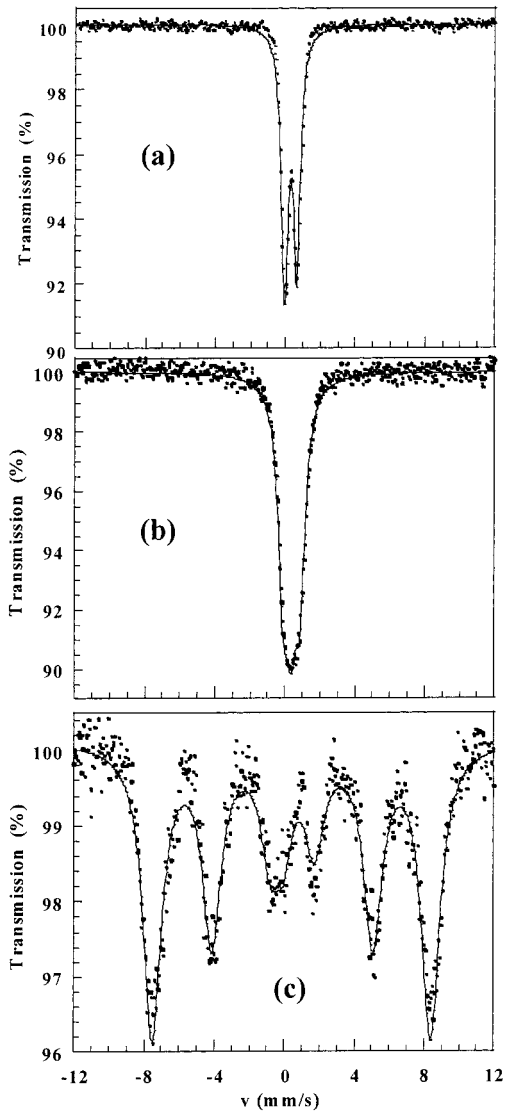

Figure 9. Mössbauer spectra of sample annealed 200 °C in air measured at (a) 290 K; (b) 77 K; (c) 4 K.

to the singlet in the sample annealed at 100 °C. The doublet disappeared in the samples annealed at 150 and 200 °C. This result shows that the doublet corresponds to the $Fe^{III}-CN-Ni^{II}$ linkage, while the singlet corresponds to the $Fe^{II}-CN-Ni^{III}$ linkage.

In the spectra of the samples annealed at 150 and 20 °C, a second doublet arose, together with the original singlet. This second doublet is certainly the characteristic subspectrum of the (Ni, Fe)$(CN)_{2-3}O_{1-2}$ structure. After annealing at 400 °C, a broad doublet appears, indicating presence of intermediate structure during the decomposition. Finally, as the annealing temperature reached 600 °C, the doublet collapsed into a sextet. In the sample annealed at 600 °C (Figure 6f), there was 8−9% of Fe atoms in a singlet. At 77 K, the singlet became a doublet and its amount was reduced. The presence of this singlet was probably due to the presence of a small amount of the metastable Fe−Ni or Fe−C compound, or due to superparamagnetism.

Chemical formulas and their Mössbauer parameters are listed in Table 2. The quantities of the individual structures measured by ambient temperature ^{57}Fe Mössbauer spectroscopy as a function of annealing temperature are tabulated in Table 3.

The Mössbauer spectra measured at different temperatures for the freeze-dried sample are shown in Figure 7a−c. The spectra taken at 290 and 77 K consist of a doublet and a singlet.

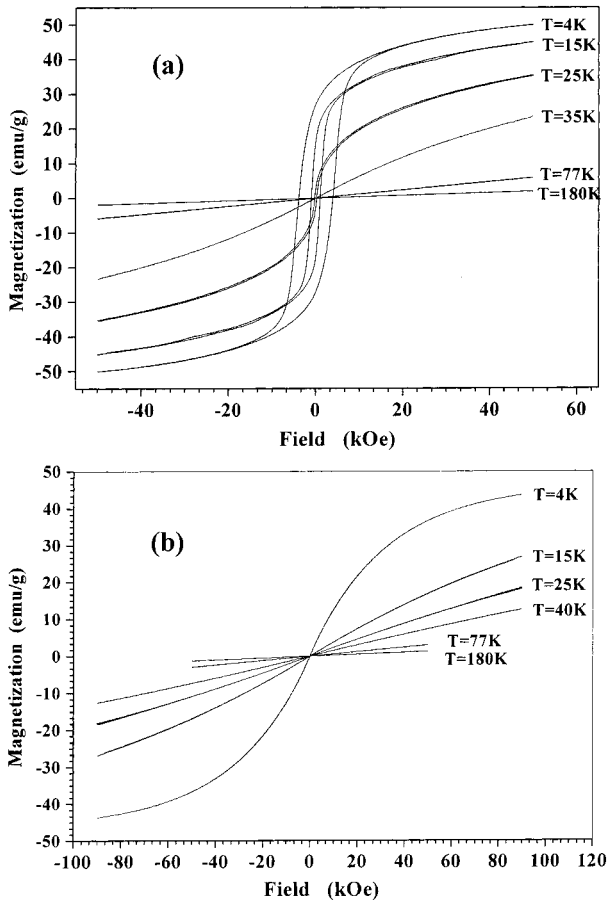

Figure 10. Magnetization curves measured by VSM as a function of temperature for (a) freeze-dried sample and (b) sample annealed at 150 °C in argon.

The first doublet that appeared in this sample corresponded to the $Fe^{III}-CN-Ni^{II}$ linkage, in which a net spin of 1/2 in the low-spin Fe^{III} ions makes the structure paramagnetic at room temperature. This doublet has a chemical shift (CS) of −0.15 mm/s and a quadrupole splitting (QS) of 0.54 mm/s. The doublet split into a sextet at 4 K, indicating that the freeze-dried sample is a magnetically ordered compound. It was found to be ferromagnetic as shall be demonstrated later.

The Mössbauer spectra of the sample annealed at 15 °C taken as a function of temperature were shown in Figure 8a−c. Only a singlet and a second doublet, which has chemically shifted to higher energy compared to the first doublet in the freeze-dried sample, were observed even at cryogenic temperatures. The singlet, with CS centered at zero, is caused by the $Fe^{II}-CN-Ni^{III}$ linkage whereby no spin exists in the low-spin Fe^{II} ion, which occupies the center of a perfect octahedron of cyanide ligands. This results in zero dipole field; therefore, no quadrupole splitting was observed. Owing to the diamagnetic property of Fe^{II} ions, the singlet was never split into a sextet even at 4 K. It is clear that the $Fe^{II}-CN-Ni^{III}$ linkage is paramagnetic throughout the whole temperature range. At 4 K, the Mössbauer spectrum became broadened, probably owing to superparamagnetism of the $Fe^{III}-CN-Ni^{II}$ and the (Fe, Ni)$(CN)_{2-3}O_{1-2}$ linkages, which were present in a small amount in the sample.

As discussed above, after annealing at 150 and 200 °C a second doublet was observed. It could be represented by the (Ni, Fe)$(CN)_{2-3}O_{1-2}$ structure. To clarify the composition, structure, and magnetic properties, it has been attempted to synthesize a sample consisting mostly of this uncertain structure. The experimental results have shown that the sample annealed

TABLE 4: Summary of the Curie−Weiss Temperature (T_c), Theoretical Magnetic Moment Per Fe(Ni) Ion ($\mu_{Fe(Ni)}$), Theoretical Magnetic Moment ($\mu_{T,Theo}$), and Experimental Magnetic Magnetic Moment (obtained by [1] fitting with Curie or Curie−Weiss Law ($\mu_{T,exp1}$); [2] Fitting with $M_{S,Exp} = N\mu_T$/Molecular Mass ($\mu_{T,exp2}$)) of the Majority Structures at Different Stages of Annealing

majority structure	treatment	T_c (K)	μ_{Fe} (μ_B)	μ_{Ni} (μ_B)	$\mu_{T,Theo}$ (μ_B)	$\mu_{T,exp1}$ (μ_B)	$\mu_{T,exp2}$ (μ_B)
$Fe^{III}-CN-Ni^{II}$	freeze-dried	28	1.7	2.8	3.6	3.6	3.8
$Fe^{II}-CN-Ni^{III}$	annealed 150 °C in argon		0	2.8	3.8	3.3	
$(Ni^{II}-Fe^{III})(CN)_{2-3}O_{1-2}$	annealed 200 °C in air	50−60				4.6	0.8

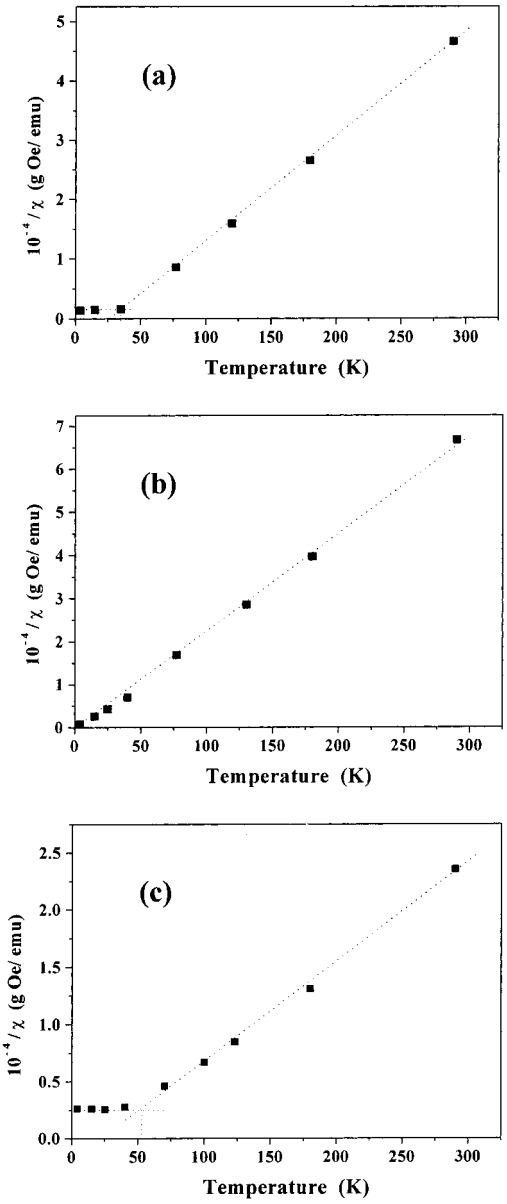

Figure 11. Temperature dependence of $1/\chi$ for samples: (a) freeze-dried; (b) annealed 150 °C in argon; (c) annealed 200 °C in air. Sample a has a transition temperature at 28 K while sample b at below K. Notice the abrupt transition at 28 K in sample a and 50−60 K in sample c. Transition temperature signifies the change from paramagnetism to ferromagnetism. $1/\chi$ was obtained from the ratio of magnetization, M (emu/g), to magnetic field, H (Oe).

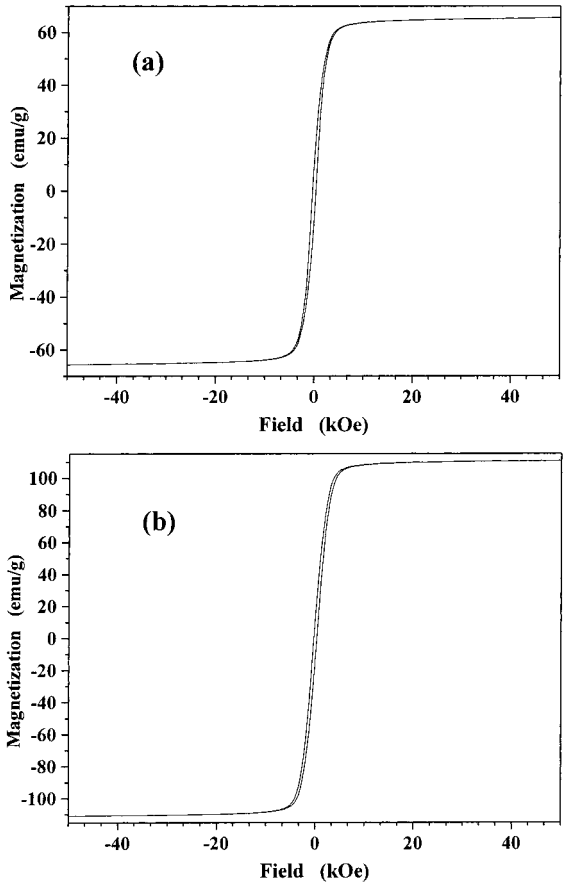

Figure 12. Magnetization curves at 290 K corresponding to ultrafine FeNi particles obtained by annealing (at 600 °C in argon), where Ni−Fe cyanides were prepared through (a) coprecipitation and (b) microemulsion.

at 200 °C in air contained 94% of the structure together with 6% of the $Fe^{II}-CN-Ni^{III}$ linkage (Table 3). Figure 9a−c shows the Mössbauer spectra of sample annealed in air at 200 °C as a function of temperature. The doublet collapsed into a sextet at 4 K with a large hyperfine field of 493 kOe, indicating that this second doublet corresponds to a magnetically ordered structure. The XRD pattern of the sample showed very broadened peaks, indicating disordered structures in this sample. The large hyperfine field observed at low temperature in the Mössbauer spectrum also suggested a significant change in the microstructure of the Fe environment. It is evident that the breaking down of some of the cyanide (CN^-) ligand bondings and the incorporation of some cyanide oxygen atoms were involved in the formation of the final product. This leads to a possible structure of (Ni, Fe)$(CN)_{2-3}O_{1-2}$ by chemical microanalysis.

For the sample annealed at 400 °C, a mixture of two structures was found from Mössbauer spectroscopy, namely, 40% of the $Fe^{II}-CN-Ni^{III}$ linkage plus 60% of the (Fe, Ni)$(CN)_x$, $x < 2$, structure. The latter structure was deduced from the chemical microanalysis. The Mössbauer parameters of the (Fe, Ni)$(CN)_x$, $x < 2$, structure are listed in Table 3. The structure is still paramagnetic at 77 K. Approximately 5% of Fe atoms were found in a magnetic sextet at 77 K with an average hyperfine field of ∼301 kOe, indicating the presence of a small amount

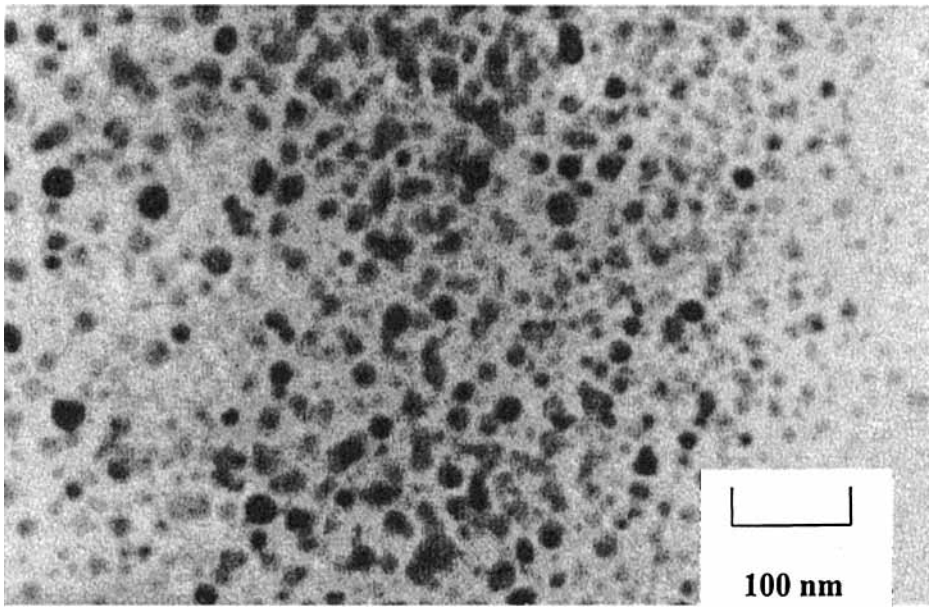

Figure 13. TEM micrograph of microemulsion-derived Fe−Ni particles after annealing of its cyanide precursor at 600 °C.

of fcc Fe−Ni. The small amount of fcc Fe−Ni might be in the ultrafine particle form. It exhibited probably superparamagnetism, because nonmagnetic sextet was not observed in the Mössbauer spectrum taken at room temperature.

Finally, a sextet with hyperfine field of 301 kOe was observed at room temperature in the sample annealed at 600 °C in argon due to the formation of fcc Fe−Ni particles from the total decomposition of the cyanide.

E. Vibrating Sample Magnetometer (VSM). Magnetization M of a magnetic substance can be described using the Langevin theory:

$$M = N\mu_T(\coth \alpha - 1/\alpha) \quad (1)$$

The function in parentheses is the Langevin function $L(\alpha)$. N denotes Avogadro's number (6.023×10^{23} mol^{-1}), μ_T the total magnetic moment of one chemical formula, and T the measurement temperature. For paramagnetism, α is $\mu_0\mu_T H/kT$, where k is the Boltzmann constant. For ferromagnetism, $\alpha = \mu_0\mu_T(H + wM)/kT$, where H is the applied magnetic field and w is the proportionality factor (the Weiss constant).

In fact, assuming magnetic quenching of the 3d orbitals in the transition metals, the theoretical value of magnetic moment μ of iron or nickel can be derived as

$$\mu_{(\text{Fe or Ni})} = g\mu_B [S_{(\text{Fe or Ni})}(S_{(\text{Fe or Ni})} + 1)]^{1/2} \quad (2)$$

where g is the gyromagnetic factor, which has been taken to be 2, and S is the total spin. So, for a single moiety such as $K_{0.8}Ni_{1.1}[Fe(CN)_6]\cdot 4.5H_2O$, the total magnetic moment is given by $\mu_{T,Theo}^2 = \mu_{Fe}^2 + (1.1\mu_{Ni})^2$. Take the freeze-dried sample, for instance; it was found from the Mössbauer spectrum to consist of 92% $Fe^{III}-CN-Ni^{II}$ linkage and 8% $Fe^{II}-CN-Ni^{III}$ linkage. Therefore, the theoretical total magnetic moment was found to be $3.6\mu_B$, from $\mu_{Fe^{III}} = 1.7\mu_B$, $\mu_{Fe^{II}} = 0$, $\mu_{Ni^{II}} = 2.8\mu_B$, $\mu_{Ni^{III}} = 3.8\mu_B$. Finally the theoretical molar saturation magnetization per unit formula is $M_{s,Theo} = N\mu_T$ (in the unit of emu/mol) $= N\mu_T/$ relative molecular mass (in the unit of emu/g).

At sufficiently low field, χ_p, the magnetic susceptibility for paramagnetic material is shown to be

$$\chi_p = N\mu_T^2/(3kT) \quad (3)$$

This is known as the Curie law where k denotes the Boltzmann constant (1.38×10^{-23} J K^{-1}).

On the other hand, the magnetic susceptibility for ferromagnetic material, χ_f, for the temperature range above its Curie−Weiss temperature (T_c), can be obtained from the Curie−Weiss law as shown below:

$$\chi_f = N\mu_T^2/[3k(T - T_c)] \quad (4)$$

By plotting the value of χ_f against T, T_c can be obtained. Once the T_c value is known, the magnetic moment per unit formula, mT, in each compound can be determined from eq 4.

Preliminary magnetic curves of the freeze-dried sample are shown in Figure 10a. In this complex compound, the ferromagnetic interaction between transition metal ions Fe and Ni through the CN^- ligands leads to a three-dimensional ferromagnetic network below T_c. From the Curie−Weiss law, T_c was estimated to be 28 K, which is very close to those reported for Ni−Fe cyanide.[9,18] Hard magnetic properties were observed in the hysteresis loops taken below the Curie−Weiss temperature. As reported previously, the coercivity was expected to be in the range of 0.7−0.9 kOe at liquid helium temperature.[17,18] The coercivity measured at 4 K was 4.0 kOe in this experiment. This high value of coercivity was due to the pure phase synthesized as well as ultrafine Fe−Ni particles in the range of 10−15 nm.

A summary of the magnetic parameters T_c, μ_{Fe}, μ_{Ni}, $\mu_{T,Theo}$, and μ_T for Fe−Ni cyanides treated at different temperatures is tabulated in Table 4. The experimental value of μ_T can also be derived from the experimental saturation magnetization $M_{s,exp}$. The value of $M_{s,exp}$ was derived from the extrapolation of M value in the plot of M versus $1/H$ with magnetic field (H) extended to infinity, using the magnetization curve measured at 4 K.

Assuming Fe^{III} and Ni^{II} ions interact ferromagnetically, using the theoretical value of magnetic moment, $\mu_{T,Theo} = 3.4\ \mu B$ (from Table 4), we obtained $M_{s,Theo} = 49$ emu/g considering a density of 2.42 g/cm3 of the freeze-dried sample. This result fitted well the experimental result of saturation magnetization, $M_{s,exp} = 55.0$ emu/g, confirming the ferromagnetism of the $Fe^{III}-CN-Ni^{II}$ linkage.

Figure 10b shows the magnetization curves taken at different temperatures for the sample annealed at 150 °C. All of the curves measured at 4−290 K were fitted well with the Langevin function for paramagnetism, giving $\mu_{T,\mathrm{Theo}} = 3.9\ \mu\mathrm{B}$. The calculated $\mu_{T,\mathrm{Theo}}$ by eq 2 with $\mu_{\mathrm{Fe^{II}}} = 0$ and $\mu_{\mathrm{Ni^{III}}} = 3.8\ \mu_{\mathrm{B}}$. This confirms the paramagnetism of the $\mathrm{Fe^{II}-CN-Ni^{III}}$ linkage. Similar patterns in magnetization curves were observed for other samples annealed at higher temperatures just below the decomposition temperature of around 250 °C. The measured magnetic moment agreed well with the theoretical values (see Table 4).

The structure corresponding to the second doublet as detected in our Mössbauer spectrum was determined to possess a transition temperature of 50−60 K by VSM measurements on the sample annealed at 200 °C in air. This structure is magnetically ordered. The measured saturation magnetization at 4.2 K was 18 emu/g by extrapolation of $M_{\mathrm{s,Exp}}$ to infinitely high field, corresponding to $\mu_{\mathrm{T}} = 0.8\ \mu\mathrm{B}$ calculated from the average chemical formula (Table 2). Using the Curie−Weiss law (Figure 10c), μT was determined to be 4.6 μB in the paramagnetic state above the magnetic transition temperature. This result indicates a ferrimagnetic arrangement of Fe and Ni ions.

In the sample annealed at 600 °C, it consisted of Fe−Ni particles, and a saturation magnetization of 66 emu/g with a coercivity of 0.35 kOe was determined from the VSM at 290 K (Figure 12a). This saturation magnetization is below the expected value of pure Ni−Fe particles ($M_{\mathrm{s,Theo}} = 100-120$ emu/g) owing to the presence of carbon particles as much as 15 wt %. Oxidation is another possible reason for the reduction of magnetization.

In a separate experiment, ultrafine magnetic powder of Fe−Ni was synthesized by the microemulsion method. The surfactant-free Fe−Ni cyanide was then annealed in 95% purity argon gas at 600 °C (i.e., oxygen is present). A saturation magnetization of 110 emu/g with a coercivity of 0.30 kOe at room temperature (Figure 12b) was found. The high value in magnetization was probably due to the reduction in pure carbon particles, owing to formation of gaseous carbon oxide. The particle size was found to be 5−10 nm in this case (Figure 13). This work has shown that the ultrafine cyanide particles may be used as the starting powder for ultrafine fine magnetic particles with a relatively high saturation. The surface is expected to be passivated owing to the presence of air. The passivated powder may have a potential for many magnetic applications, e.g., magnetic recording.

IV. Conclusion

The low-temperature molecular magnet nickel−iron cyanide powder was prepared by the coprecipitation method where the particle size is in the nanoscale range. It possessed an fcc crystal structure with lattice parameter of around 10 Å. This ferromagnetic powder has a Curie temperature of 28 K. The effects of annealing on its physical as well as magnetic properties were studied. The $\mathrm{Fe^{III}-CN-Ni^{II}}$ linkage is the major structure in the freeze-dried Ni−Fe cyanide. As the cyanide was annealed up to 150 °C, a second major linkage appeared, namely, $\mathrm{Fe^{II}-CN-Ni^{III}}$. Owing to its lower total spins in the latter sample, it leads to a decline in the saturation magnetization in the transition-metal cyanide powder. As annealing temperature is increased, another disordered structure in the cyanide was observed, namely, $\mathrm{(Ni, Fe)(CN)_{2-3}O_{1-2}}$. Decomposition of the cyanide began beyond 250 °C. This involved the loss of some cyanide ligand bondings, leading to structures such as $\mathrm{(Ni, Fe)(CN)_{\mathit{x}}}$, $x < 2$. It was completely decomposed above 550 °C, whereby nanoscale Fe−Ni particles were found, as well as a minor amount of iron carbide and carbon particles. Annealing at 600 °C under an argon/air mixture atmosphere lead to formation of fairly pure Fe−Ni particles with particle sizes of 5−10 nm and a saturation magnetization of 110 emu/g with a coercivity of 0.3 kOe.

References and Notes

(1) Turnbull, M. M.; Sugimoto, T.; Thompson, L. K. In *Molecule-Based Magnetic Materials−Theory, Techniques and Applications*; American Chemical Society: Washington, D.C., 1996.

(2) Miyasaka, H.; Matsumoto, N.; Okawa, H.; Re, N.; Gallo, E.; Floriani, C. *J. Am. Chem. Soc.* **1996**, *118*, 981.

(3) Stumpf, H. O. *Science* **1993**, *261*, 447.

(4) Ferlay, S.; Mallah, T.; Ouahes, R.; Veillet, P.; Verdaguer, M. *Nature* **1995**, *378*, 701.

(5) Mallah, T.; Thiebaut, S.; Verdaguer, M.; Veillet, P. *Science* **1993**, *262*, 1554.

(6) Marvilliers, A.; Mallah, T.; Riviere, E. *Mol. Cryst. Liq. Cryst. A: Part 2*, **1999**, *334*, 1195.

(7) Mallah, T.; Ferlay, S.; Aubeger, C. *Mol. Cryst. Liq. Cryst. A* **1995**, *273*, 141.

(8) Ziolo, R. F.; Giannelis, E. P.; Weinstein, B.; O'Horo, M. P.; Ganguy, B. N.; Mehrotra, N.; Russell, M. W.; Huffamn, D. R. *Science* **1991**, *257*, 219.

(9) Kahn, O. In *Molecular Magnetism: From Molecular Assemblies to the Devices*; Goronado, E., Delhaés, P., Gatteschi, D., Miller, J. S., Eds.; Nato ASI Series E: Applied Science 321; Kluwer Academic Publishers: Norwell, MA, 1996; p 243.

(10) Larionova, J.; Kahn, O.; Goldhen, S. *Mol. Cryst. Liq. Cryst. A: Part 1* **1999**, *334*, 651.

(11) Sato, O.; Einaga, Y.; Fujishima, A.; Hashimoto, K. *Inorg. Chem.* **1999**, *38*, 4405.

(12) Yokoyama, T.; Kiguchi, M.; Ohta, T.; Sato, O.; Einaga, Y.; Hashimoto, K. *Phys. Rev. B* **1999**, ***60***, 9340.

(13) Einaga, Y.; Sato, O.; Iyoda, T.; Fujishima, A.; Hashimoto, K. *J. Am. Chem. Soc.* **1999**, **121**, 3745.

(14) Kahm, O. *Nature* **1999**, *399*, 6731.

(15) Kahm, O. *Nature* **1995**, *378*, 6558.

(16) Inoue, K.; Koga, N.; Iwamura, H. *J. Am. Chem. Soc.* **1991**, *113*, 9803.

(17) *Infrared and Raman Spectra of Inorganic and Coordination Compounds, Part B: Applications in Coordination, Organometallic and Bioorganic Chemistry*, 5th ed.; Nakamoto, K, Ed.; Wiley Interscience: New York, 1997.

(18) Juszczyk, S.; Johansson, C.; Hanson, M.; Ratuszna, A.; Malecki, G. *J. Phys.: Condens. Matter* **1994**, *6*, 5697.

(19) Ng, C. W.; Ding, J.; Chow, P. Y.; Ganand, L. M.; Quek, C. H. *J. Appl. Phys.* **2000**, *87*, 6049.